CNRS
Centre National de la Recherche Scientifique

INFN
Istituto Nazionale di Fisica Nucleare

Advanced Virgo Length Sensing and Control steady state design

VIR-0738A-11

Gabriele Vajente
INFN Sezione di Pisa

Issue: A

Date: December 20, 2011

VIRGO * A joint CNRS-INFN Project
Via E. Amaldi, I-56021 S. Stefano a Macerata - Cascina (Pisa)
Secretariat: Telephone (39) 050 752 521 * FAX (39) 050 752 550 * Email W3@virgo.infn.it

Contents

1 Introduction

This note describes the design of the steady state length sensing and control (LSC) scheme for Advanced Virgo. The optical configuration is the one described in [1]. The main parameters are summarized in tab. 1. This work substitutes and integrates what described in the previous notes [2]. The optical response of the interferometer has been simulated using Optickle [3] which is as of today the only tool capable of including radiation pressure effects.

Three different configurations have been considered for all the design steps: power-recycled only interferometer at low input power, namely 25 W; dual recycled interferometer at low input power (25 W); dual recycled interferometer at full input power, namely 125 W.

2 Definition of degrees of freedom

In a dual recycled interferometer the length sensing and control system deals with five degrees of freedom. Referring to fig. 1, the microscopic positions (*tunings*) of all mirrors are combined to obtain the following physical degrees of freedom:

$$\begin{aligned} DARM &= L_N - L_W \\ CARM &= \frac{L_N + L_W}{2} \\ MICH &= l_N - l_W \\ PRCL &= l_P + \frac{l_N + l_W}{2} \\ SRCL &= l_S + \frac{l_N + l_W}{2} \end{aligned}$$

Parameter	**Value**
Power recycling mirror transmission	0.05
Input mirror transmission	0.014
End mirror transmission	1 ppm
Signal recycling mirror transmission	0.2
Losses per mirror	32.5 ppm
Arm cavity mirror mass	42 kg
Power recycling cavity length	11.952 m
Signal recycling cavity length	11.952 m
Schnupp asymmetry	0.23 m
Arm cavity length	2999.8 m
Modulation frequencies	$f_1 = 6270777$ Hz
	$f_2 = 56436993$ Hz
	$f_3 = 8361012$ Hz
Suspension last stage resonant frequency	600 mHz
DC readout offset	such to have 80 mW on dark fringe after OMC
Signal recycling cavity detuning	3.022×10^{-7} m

Table 1: List of relevant parameters used in the Optickle simulation. Reference from [1].

Mirror motions are defined to be orthogonal to the mirror surface, in a direction defined by the following convention:

- PRM motion is positive in BS direction
- SRM motion is positive in BS direction
- BS motion is positive in PRM direction
- NE and WE motions are positive when cavities get shorter

The simplest extension of Virgo driving to AdVirgo consists in controlling MICH / PRCL / SRCL using PRM / SRM / BS. The following relations between mirror motions and lengths hold:

$$\begin{aligned} \delta l_P &= \delta z_{PRM} - 2\delta z_{BS} \\ \delta l_N &= \sqrt{2\delta z_{BS}} \\ \delta l_W &= 0 \\ \delta l_S &= -\delta z_{SRM} \end{aligned}$$

These equations can be inverted to obtain the driving matrix for longitudinal control, namely the relation between corrections in degrees of freedom basis and mirror basis:

$$\begin{aligned} \delta z_{NE} &= -\frac{DARM}{2} - CARM \\ \delta z_{WE} &= +\frac{DARM}{2} - CARM \\ \delta z_{BS} &= \frac{1}{\sqrt{2}} MICH \\ \delta z_{PRM} &= -PRCL - \frac{1}{2} MICH \\ \delta z_{SRM} &= -SRCL + \frac{1}{2} MICH \end{aligned}$$

Table 2 summarizes the driving matrix for a dual recycled interferometer as it is used in all the following simulations.

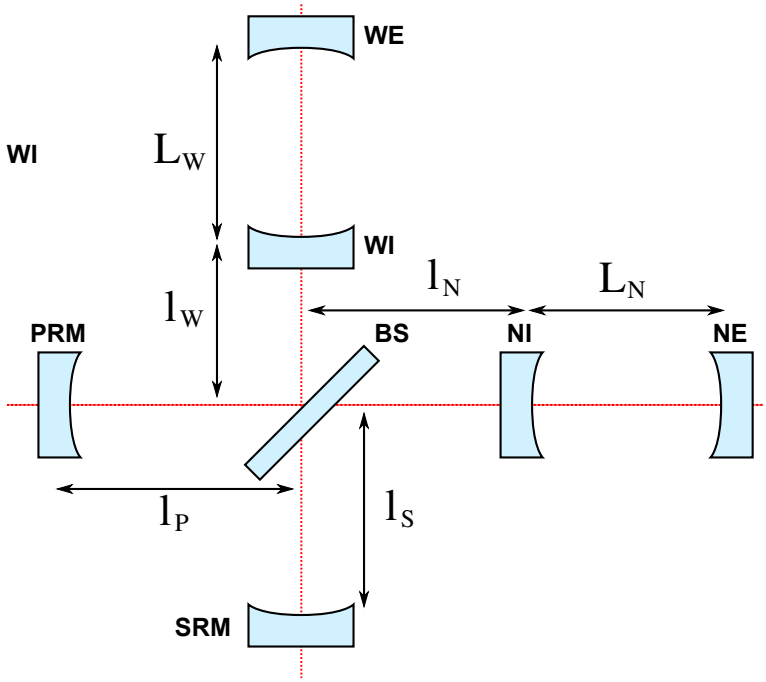

Figure 1: Scheme of relevant physical distances between mirrors in a dual recycled interferometer.

Mirror/DOF	DARM	CARM	MICH	PRCL	SRCL
NE	$-1/2$	-1			
WE	$1/2$	-1			
BS			$1/\sqrt{2}$		
PRM			$-1/2$	-1	
SRM			$1/2$		-1

Table 2: Driving coefficients for dual recycled interferometer.

In addition to these "mechanical" degrees of freedom one should consider the laser frequency stabilization loop, which locks the laser to the mean length of the two arm cavities with typical band-widths of few tens of kHz.

3 Definition of available output ports and signals

There are many output ports foreseen in Advanced Virgo:

- The dark fringe or asymmetric port: before the output mode cleaner a small fraction is extracted and sent to B1p. The transmission of the OMC is B1 and the reflection is B1s. Since the OMC should filter all sidebands, B1 contains only the fundamental mode carrier field, while all high order modes and sidebands should therefore go in B1s. For steady state longitudinal control only B1 is used.
- The interferometer reflection or symmetric port, named B2. The amount of power available in this port depends largely on the impendence matching between the PR mirror and the arm cavities reflectivities, which is in turn determined by their round trip losses.
- The transmission of the two arm cavities, named B7 and B8 for north and west respectively. These port will not receive a lot of light since the end mirror transmission is expected to be very small. They will not be used for the steady state control.

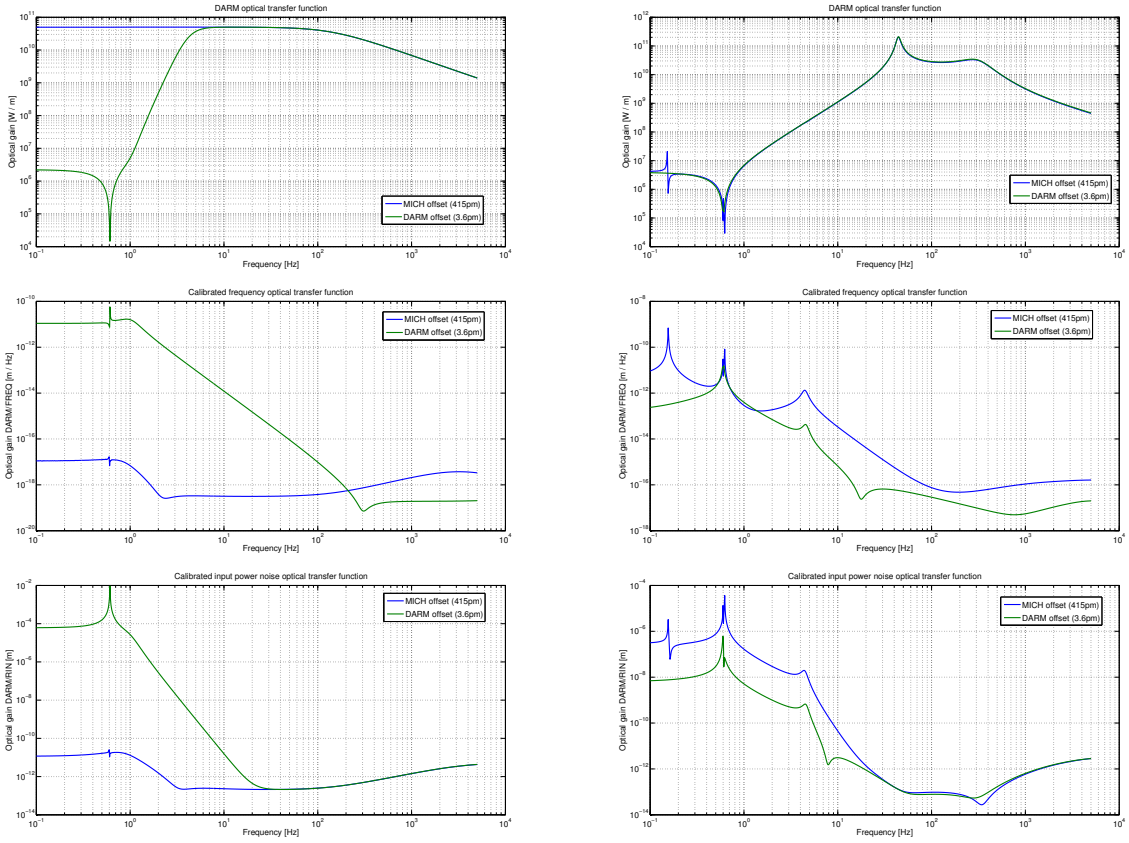

Figure 2: Comparison of optical transfer function with MICH or DARM offsets, in the case of power recycled (left) or dual recycled interferometer (right). Top plot shows the DARM optical transfer function (coupling of DARM to dark port power). Middle plot shows the coupling of frequency noise to DARM (calibrated dark port power). Bottom plot the coupling of power noise.

- The power recycling cavity pick-off port, which will be extracted using a plate in front of the power recycling mirror. The reflectivity of this plate should be about 300 ppm in order to be able to extract enough power in this beam for angular and longitudinal control, even in low power configurations.

The beam is frontal modulated at three radio frequencies listed in tab. 1, using electro-optical modulators placed before the input mode cleaner, with modulation indexes set to 0.1. The frequencies must therefore be multiples of the IMC free spectral range. These frequencies are listed in tab. 1. Not all the possible demodulated signals will be needed at all ports: B1 beam will not see any sideband, so demodulation is useless on that port; f_3 is anti-resonant in the recycling cavity, so signals demodulated at this frequency will be useful only in B2 beam; B5 beam finally will contain both f_1 and f_2 sidebands and will provide useful signals at both demodulations. The name convention used in this note for signal is: PORT_SBx_yy where x refer to the modulation frequency and can range from 1 to 3, while yy can be DC, P or Q referring respectively to power signal, demodulated in-phase and demodulated quadrature channels. Demodulation phase is chosen in each configuration in order to maximize one chosen degree of freedom in P over Q. Details are given for each configuration separately.

The total power which is sensed at each longitudinal photo-diode is 100 mW, accordingly to specifications given by the DET subsystem. All signals are assumed to be dominated by shot noise.

Configuration	DOF	Offset [m]
Power recycled 25W	MICH	$1.6 \cdot 10^{-9}$
Dual recycled 25W	DARM	$2.3 \cdot 10^{-11}$
Dual recycled 125W	DARM	$1.0 \cdot 10^{-11}$

Table 3: Offsets needed for reaching 80 mW of power at dark port.

Configuration	DARM	Frequency	CARM	MICH	PRCL	SRCL
Power recycled 25W	$6 \cdot 10^{-16}$ m	7 mHz	$4 \cdot 10^{-13}$ m	$2 \cdot 10^{-13}$ m	2×10^{-11} m	n.d.
Dual recycled 25W	$2 \cdot 10^{-15}$ m			$6 \cdot 10^{-13}$ m		3×10^{-12} m
Dual recycled 125W	$1 \cdot 10^{-15}$ m			$3 \cdot 10^{-13}$ m		

Table 4: Summary of accuracy requirements for longitudinal control loops.

4 DC readout offset

The DC-readout scheme foresees the addition of an offset to a differential degree of freedom, in order to have a static carrier field reaching the dark port, to be used as phase reference for homodyne detection. In principle it is possible to generate such a static field both with an offset in DARM or MICH. The use of a DARM offset introduces a detuning of the arm cavities from resonance, thus in principle increasing the influence of radiation pressure. Instead using a MICH offset does not move the arm cavities out of resonance. In the presence of a signal recycling cavity the distinction is however not clear. One important point is how optical transfer functions change with the offset, in particular the DARM one and the power and frequency noise couplings.

Plots in the left side of figure 2 compares the result of Optickle simulation in the two cases for a power recycled interferometer. MICH and DARM offsets have been added separately, resulting in the same amount of carrier power reaching the dark port. The first plot shows that if the offset is added to MICH instead of DARM, there is no more any effect of radiation pressure in the DARM optical transfer function. Moreover, in the case of MICH offset, the coupling of frequency and power noises to the output signal is lower, at least in the more critical low frequency region. Therefore the use of a MICH offset is preferable in the case of power recycled only interferometer.

The situation is different in the dual recycled case, as shown in the right plots of figure 2. Since the DARM optical transfer function is dominated by radiation pressure effects due to the signal recycling cavity, there is no difference wherever the offset is added. Frequency and power noises instead couple more if a MICH offset is used. It is then preferable to use a DARM offset in the dual recycled case.

In conclusion, in the following simulations, a MICH offset is used in the power recycled interferometer and a DARM one in the dual recycled case.

In all three configuration the offset is tuned in order to have 80 mW of carrier TEM00 power at dark port. The resulting offsets are summarized in table 3.

5 Accuracy requirements

First requirements on the desired final accuracy for the longitudinal control loops have been already computed in [2]. Some of those computations are updated here. The final requirements are summarized in tab. 4.

DARM

Some requirements on residual DARM motion can come from consideration on the line-width of the arm cavity, which is of the order of

$$\delta z = \frac{\lambda}{4\mathcal{F}} \sim 6 \times 10^{-10} \text{ m} \tag{1}$$

However the most stringent requirement comes from the use of DC readout. Indeed the response of the dark fringe power to differential motion is intrinsically non-linear: the DC power at B1 varies with very good approximation as a parabola centered at zero offset. The optical gain is given by the derivative of this parabola and therefore it varies linearly even around the operating point, which is defined as the one giving 80 mW of power.

In general the power at dark port can be described by the following equation:

$$B1 = A + Bz^2 \tag{2}$$

where z is the full DARM displacement from resonance, including the DC readout offset. The coefficients A and B can be obtained from simulations. Around the working point one can write $z = z_0 + \delta z$ where z_0 is the static offset and δz is the residual motion of DARM:

$$\begin{aligned} B1 &= A + B(z_0 + \delta z)^2 \\ &= A + Bz_0^2 + 2Bz_0 \cdot \delta z + B\delta z^2 \\ &= b_0 + \alpha\delta z + \beta\delta z^2 \end{aligned} \tag{3}$$

where the last line gives the definition of b_0, α and β.

One of the effects of the non-linear term in the DARM motion is to create up-conversion of low frequency residual DARM motion around high frequency lines. Indeed, the previous equations are correct in the time domain:

$$b(t) = b_0 + \alpha\delta z(t) + \beta\delta z(t)^2 \tag{4}$$

which in frequency domain becomes:

$$\tilde{b}(f) = \alpha\tilde{\delta z}(f) + \beta(\tilde{\delta z} \star \tilde{\delta z})(f) \tag{5}$$

If we assume the DARM motion to be composed of a low frequency part (residual motion) and of a large spectral line (like for example violin modes):

$$\tilde{\delta z}(f) = z_{RMS}\delta(f) + z_L\delta(f - f_L) \tag{6}$$

the convolution can be easily computed and the signal on the diode at the line frequency will be

$$\tilde{b}(f) = \alpha z_L \left(1 + \frac{2\beta}{\alpha} z_{RMS}\right) \delta(f - f_L) \tag{7}$$

The second term inside the brackets gives the level of low frequency up-converted noise which falls around the main line. This noise couples directly to the detector sensitivity, thus it must be required to be a factor 10 below the design sensitivity. Assuming to have lines with a SNR of 1000, which is typical of violin and mirror modes, the term must satisfy:

$$\frac{2\beta}{\alpha} z_{RMS} < \frac{1}{10} \cdot \frac{1}{1000} = 10^{-4} \tag{8}$$

From equation 3 one can substitute α and β and finally find the following relation which gives the requirement for DARM:

$$\frac{z_{RMS}}{z_0} < 10^{-4} \tag{9}$$

which means that the DARM accuracy must be a factor 10^4 smaller than the actual offset needed to get 80 mW at dark port. This means that for power recycled only configuration at 25W DARM accuracy must be at the level of $6 \cdot 10^{-16}$ m; for dual recycled at 25 W at $2 \cdot 10^{-15}$ m; for dual recycled at 125 W at $1 \cdot 10^{-15}$ m.

MICH

Residual motion of the MICH degree of freedom is in first approximation equivalent to a DARM one, provided the scaling factor of the arm cavity optical gain is taken into account: $2\mathcal{F}/\pi \sim 280$. This result in a requirement of the order of $2 \cdot 10^{-13}$ m in power recycled 25 W configuration; $6 \cdot 10^{-13}$ m in dual recycled 25 W configuration; $3 \cdot 10^{-13}$ m in dual recycled 125 W configuration.

PRCL

For PRCL one can consider the resonance width of the cavity for the carrier. A recycling gain of the order of 70 corresponds to a finesse of 110 and a line-width of 2×10^{-9} m. If we require the fluctuations to be at least 100 times smaller than the line-width we obtain a requirement of about 2×10^{-11} m. This requirement is independent of the ITF configuration.

Frequency stabilization and CARM

A motion of CARM causes a phase rotation in reflection of the cavity which is equivalent to a PRCL displacement. Therefore a requirement for CARM can be obtained rescaling the PRCL one by the optical gain of the Fabry-Perot cavities. The results is 7×10^{-14} m or correspondingly 7 mHz in term of residual laser frequency fluctuation on the time scale of seconds, with respect to the arm cavity length reference.

The very low frequency absolute fluctuation of the laser frequency is dominated by the residual motion of the arm cavity mean length. This is at first order not relevant for the interferometer except for the presence of the output mode cleaner. Indeed any fluctuation of the laser frequency will be equivalent to a change in the length of the OMC and will at some level spoil its lock accuracy. If an accuracy δz_{OMC} is needed for avoid the re-introduction of OMC length noise in the sensitivity [4, 5, 6], the corresponding tolerable residual motion of the mean arm length is given by

$$\delta z_{CARM} \sim \frac{L_{ARM}}{L_{OMC}} \cdot \delta z_{OMC} \tag{10}$$

Assuming a length of the OMC of about 30 cm [6], a level of length noise of the OMC of the order of $4 \cdot 10^{-17}$ m/$\sqrt{\text{Hz}}$ at 10 Hz, the required accuracy for OMC lock is of the order of $4 \cdot 10^{-13}$ m. This corresponds to a CARM lock accuracy of $4 \cdot 10^{-9}$ m or 400 Hz in term of laser frequency. The CARM slow loop will use, as in Virgo, an error signal in reflection of the reference cavity, with typical bandwidths of few Hz.

SRCL

In the case of the signal recycling cavity the requirement should come from the stability of the optical response of the interferometer. It should not change more than a given small factor inside the detection band due to residual motion of the cavity length. Simulations show that the optical response changes less than 1% when the SRCL accuracy is better than 3×10^{-11} m. Requiring a variation lower than 10^{-3} reduced the allowed residual motion to 3×10^{-12} m. See figure 3 for the simulation outcome.

5.1 Consequences of the accuracy requirements on OMC filtering

In an ideal world only the carrier fundamental mode is transmitted by the output mode cleaner. However in reality parts of the sidebands and of high order modes are also leaking through the OMC. If these leakage fields fluctuate in amplitude, they will give rise to spurious power fluctuations of the dark fringe photo-diode which will be interpreted by the DARM loop as a motion of the physical degree of freedom.

The maximum leakage power which is tolerable depends on the required DARM accuracy and on the expected power fluctuation of the leaking field. The latter is quite difficult to predict. However a reasonable estimate

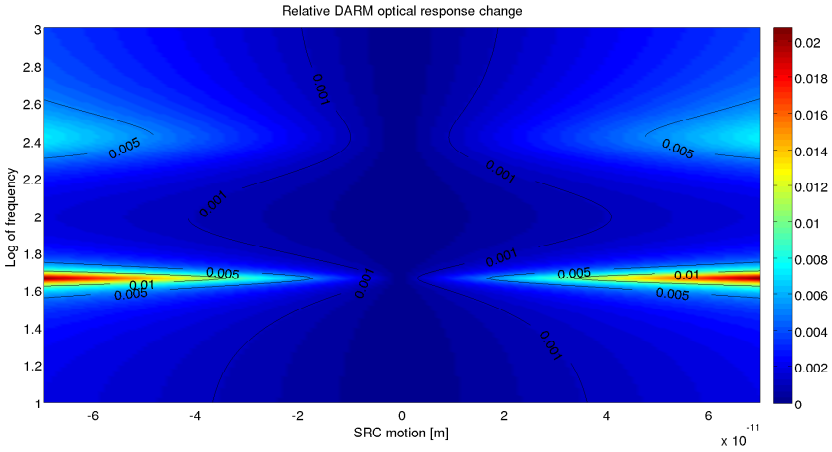

Figure 3: Variation of detector response as a function of signal recycling motion around nominal point and frequency.

can be obtained looking at the residual intensity fluctuation of sideband fields at the dark port during the last Virgo+ science run. It turns out that sideband power fluctuates typically of about 2%, coherently with interferometer motions especially in the micro-seismic region.

Since at low frequency (below about 1 Hz) the DARM loop has very high gain, any spurious power fluctuation at the dark port is directly converted into a real motion of the DARM degree of freedom, with a conversion factor given by the *purely optical* transfer function of the interferometer. This spurious motion of DARM induced by the loop is not measurable in any way, since the error signal will be squeezed to zero by the high loop gain.

The word purely optical in the last paragraph is relevant when in a radiation pressure dominated regime. Radiation pressure create an opto-mechanical modification of the transfer function. Any force applied to the DARM degree of freedom creates a potential displacement of the same degree of freedom. This in turn modulates the field inside the arms and via radiation pressure this induces an additional force on DARM. The net effect is a reduced real motion of the degree of freedom. However, once the real displacement is properly computed, taking into account the depressing factor due to radiation pressure, the dark fringe power signal responds with a transfer function which depends only on the optics and corresponds to what one would get from computations which do not include radiation pressure.

The spurious DARM motion induced by a leakage field residual intensity noise is given by

$$\delta_{DARM} = \frac{P_s RIN_s}{G} \tag{11}$$

where G is the optical gain of dark fringe with respect to DARM; P_S is the total power of the leaking field and RIN_S is the corresponding residual intensity noise.

To properly control the DARM loop at the level of accuracy δz_{RMS} considered in the previous section, the contribution of spurious motion due to leaking field must be well below this level. If we ask this contribution to sum up to less than 10% of the needed accuracy, the limit on leaking field is given by:

$$P_S < \frac{1}{10} \cdot \frac{\delta z_{RMS} G}{RIN_S} \tag{12}$$

The resulting requirements on leaking power in transmission of the dark fringe are summarized in tab. 5 as a function of the interferometer configuration.

Configuration	Optical gain (G)	Requirements
Power recycled 25W	$2.8 \cdot 10^{10} W/m$	0.08 mW
Dual recycled 25W	$7 \cdot 10^{9} W/m$	0.07 mW
Dual recycled 125W	$1.5 \cdot 10^{9} W/m$	0.08 mW

Table 5: Requirement on spurious field transmission through the OMC, assuming a residual intensity noise of 2%.

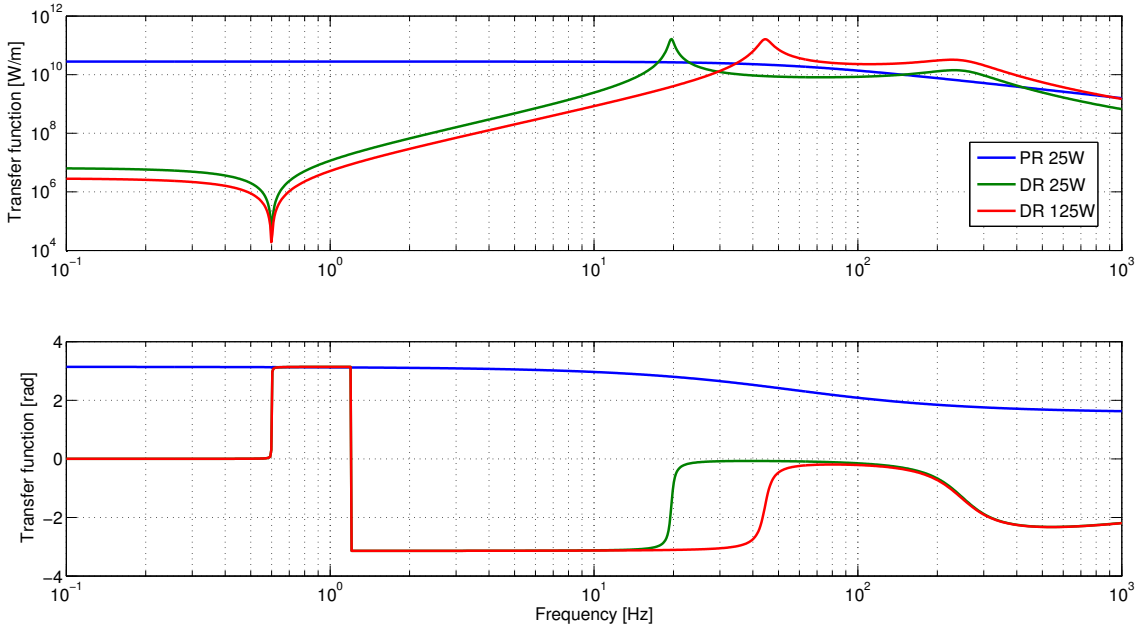

Figure 4: Shape of the dark fringe photo-diode DC signal response to DARM motion.

6 Response of dark fringe to differential motion

The response of the interferometer to motions of any degree of freedom is simulated using Optickle [3] which is so far the only simulation tool capable of properly include radiation pressure effects. The transfer function which is most affected, at least in the dual recycled case, is the DARM one. The outcome of Optickle simulation has been fitted to obtain a list of zeros and poles to properly describe the dynamical properties of the interferometer response. Figure 4 shows the shape of such transfer function in the different configurations, while tab. 6 lists the result of the fitting procedure. These are the transfer functions from the mirror suspension point displacement to mirror motion, including the effect of radiation pressure induced optical springs. To obtain the response of the degree of freedom to a force applied directly to the mirror by the actuators one should multiply by the pendulum response.

7 Design and performances of the longitudinal controls

For all configurations the control loop simulation has been obtained using the following procedure.

1. The DARM offset is set accordingly to table 3 in order to have 80 mW at the dark port diode.
2. A frequency domain Optickle simulation of the entire interferometer is run, and the transfer functions

Configuration	DARM transfer function
Power recycled 25W	$\frac{-2.36 \cdot 10^{11}}{(s+355.1)(s^2+0.00770s+14.21)}$
Dual recycled 25W	$\frac{6.85 \cdot 10^{10}(s+5945)}{(s^2-5.25s+1.52e04)(s^2+828s+2.45e06)}$
Dual recycled 125W	$\frac{1.51 \cdot 10^{11}(s+6000)}{(s^2-28.2s+7.80e04)(s^2+849s+2.41e06)}$

Table 6: Transfer function from DARM motion to dark fringe diode DC power, in W/m. $s = 2i\pi f$ is the Laplace variable.

from each degree of freedom to each photo-diode signal are extracted.

3. For each degree of freedom the best error signal is searched for, looking for the one that maximizes the signal to noise ratio. Demodulation phases are tuned in order to maximize the signal in P over Q for the corresponding degree of freedom.

The transfer functions of all central interferometer degrees of freedom show complex frequency dependencies due to radiation pressure effects [7]. These affects mainly the carrier field which contributes to demodulated signals. To cope with these effects control loops are closed in two stages.

4. The DARM and frequency stabilization optical transfer functions are fitted using MATLAB and the Vector Fitting algorithm [8].
5. Stable controllers are developed for DARM and frequency stabilization separately.
6. The effect of closing only DARM and frequency stabilization loops is simulated with MATLAB, with particular care to extract the resulting optical transfer function of the central interferometer degrees of freedom.

In this way, once DARM and frequency loops are closed, there are no more radiation pressure effects in the transfer functions of MICH, PRCL and SRCL.

7. MICH, PRCL and SRCL optical transfer functions can be modeled very well with constant gains, which are again extracted from the previous simulation.
8. Stable controllers are developed for these degrees of freedom.
9. All control loops are then closed all together and the coupling of the sensing noise of each degree of freedom to the dark fringe signal is computed and calibrated in terms of the detector sensitivity.
10. Typically all control noises are well above the design sensitivity. Therefore proper noise subtraction paths [9] must be implemented, adding a off-diagonal term in the driving matrix. This is equivalent to what in Virgo was called alpha technique which corresponded to adding a filtered version of the MICH correction to the DARM one, in order to cancel as much as possible the direct optical coupling. In Virgo noise coupling reductions of the order of 500 was achieved. This is the same level assumed as feasible in Advanced Virgo and used in all the following simulations.
11. The sensing noise introduced by the loop in the detector sensitivities is required to stay a factor 10 below the design sensitivity. If this is not the case an optimization of the controller is needed, starting again from step 7 above.
12. The loop performance in term of accuracy is estimated, computing the residual motion of all degrees of freedom. The starting point is an estimation of the free motion of each mirror obtained analyzing the correction sent to the power recycling mirror during Virgo+ last run. A calibrated version of the correction signal is used to estimate the free motion below 1 Hz, while above a power law scaling is assumed. However

most of the RMS in closed loop configuration come from frequencies below 1 Hz, so higher frequencies does not really matter too much. The free motion corresponds to a total RMS of about 0.2 μm.

13. The resulting accuracies are compared to the corresponding requirements. If they are not compliant, the controller must be optimized, keeping also an eye on noise introduction, starting again from step 7 above.

It turned out during the optimization of the filters that a large coupling between degrees of freedom (mainly MICH and DARM) is present, mainly at low frequency. To be able to reach the desired accuracy a proper decoupling of the loops must be achieved by measuring and inverting the sensing matrix. The precision needed for such inversion ranges from 10% in the power recycling case to fractions of 1% in the dual recycling case, which is a quite difficult performance to achieve. More investigations in this directions will be needed.

7.1 Power recycled 25 W

As anticipated in section 4 in the power recycled configuration the DC readout offset is added to the MICH degrees of freedom. Its value, as show in tab. 3 is $1.6 \cdot 10^{-9}$ m. The characteristics of the control filters are summarized in tab. 7. Note that the interferometer response to laser frequency has not been simulated completely above 5 kHz. This means that the frequency stabilization control filter must include, in addition to the singularities shown in the mentioned table, also some shaping to compensate the optical one around few tens of kHz.

The signals used to control each degree of freedom are listed in tab. 8.

The performances in terms of control noise injection are shown in figure 5, where noise subtraction loops are implemented with a reduction factor of 500. In the case of PRCL and CARM (frequency noise) the noise coupling is likely underestimated, since no defect nor asymmetries have been added to the interferometer. The MICH loop is the most critical one and its contribution is just at the level of the 1/10 safety factor. Any increase of sensing noise with respect to shot noise in this configuration will result in the longitudinal control not being compliant with the requirements.

The accuracies of the loop are summarized in tab. 8. All loops are compliant with the requirements.

7.2 Dual recycled 25 W

In dual recycled configuration the DC readout offset is added to the DARM degree of freedom and it has a value of $2.3 \cdot 10^{-11}$ in order to have 80 mW of carrier power reaching the dark port. The characteristics of the control filters are summarized in tab. 9. Note that the interferometer response to laser frequency has not been simulated completely above 5 kHz. This means that the frequency stabilization control filter must include, in addition to the singularities shown in the mentioned table, also some shaping to compensate the optical one around few tens of kHz.

The signals used to control each degree of freedom are listed in tab. 10.

In the dual recycled case the DARM loop is forced to have a quite high bandwidth (400 Hz in this case) in order to properly stabilize the unstable optical spring generated by the interplay between the DC readout offset and the signal recycling cavity. Note that the computation of phase margin does not include the effect of any delay introduced by the DAQ system. The effect can be significant at these high unity gain frequencies.

Figure 6 shows the sensing noise introduced in the detector sensitivity by the longitudinal control loops. Again the MICH loop is very close to the 1/10 safety factor below design sensitivity. Any increase of sensing noise with respect to shot noise in this configuration will result in the longitudinal control not being compliant with the requirements.

The accuracies of the loop are summarized in tab. 10. All loops are compliant with the requirements.

D.O.F.	Control filter	UGF	Gain mar.	Ph. mar.
DARM	$-0.02129\frac{(s+38.95)(s+17.4)^2(s+224.7)(s^2+30.5s+1239)(s^2+184.6s+1.14\cdot10^4)}{s^2(s+2640)(s+2256)(s+0.6084)^2(s^2+2.501s+37.44)}$	100 Hz	11 db	42 deg.
Freq.	$1.69\cdot10^{17}\frac{(s+3.527\cdot10^4)^2}{s(s+7.053\cdot10^5)^2(s+62.59)}$	26 kHz	16 db	39 deg.
MICH	$-4180\frac{(s+6.276)(s+6.575)(s+4.266)^2(s+15.83)(s^2+6.775s+125.8)}{s^2(s+265)(s+358.7)(s+0.06575)(s+0.04294)(s^2+2.042s+1.851)}$	13 Hz	16 db	29 deg.
PRCL	$-8.1\cdot10^5\frac{(s+20.13)(s+24.24)^2(s+30.8)(s+33.32)^2(s+34.15)(s+66.38)}{s^2(s+510.2)^2(s+1105)(s+1259)(s^2+0.7034s+0.3933)(s^2+1.204s+10.54)}$	40 Hz	6 db	40 deg.

Table 7: Control filters in the power recycled 25 W configuration.

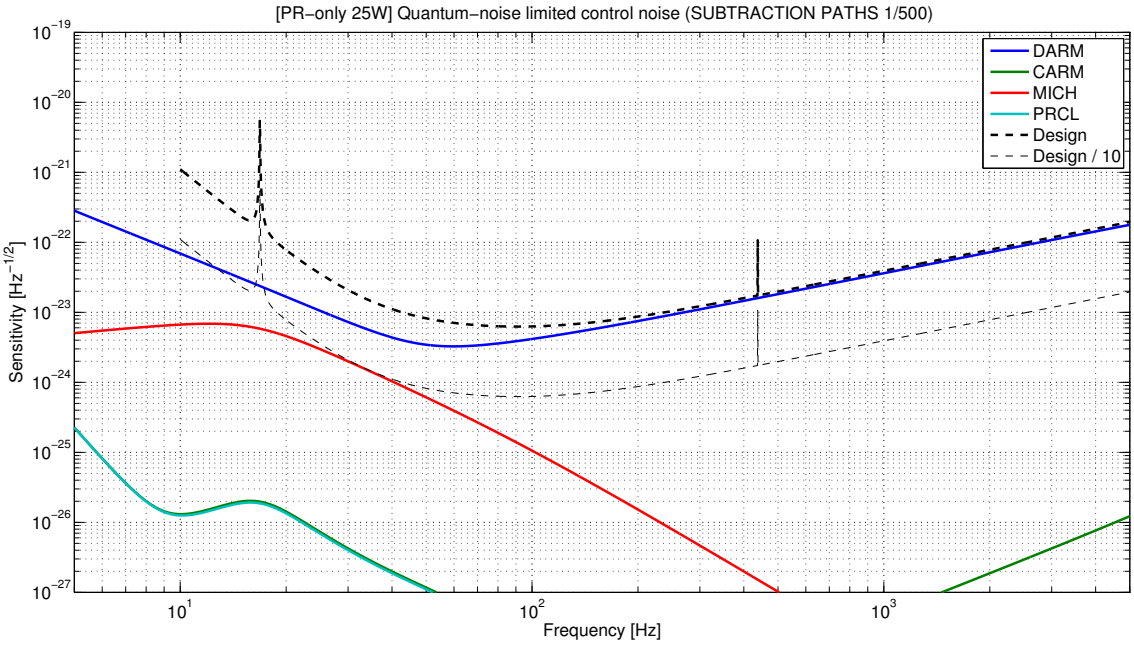

Figure 5: Sensing noise re-introduced in the detector sensitivity by longitudinal control loops in the power recycled configuration with 25 W input power.

D.O.F.	Error signal	Accuracy	Requirement
DARM	B1_DC	$5 \cdot 10^{-16}$ m	$6 \cdot 10^{-16}$ m
Frequency	B2_SB1_P	0.6 mHz	7 mHz
MICH	B5_SB1_Q	$1.3 \cdot 10^{-13}$ m	$2 \cdot 10^{-13}$ m
PRCL	B2_SB3_P	2×10^{-12} m	2×10^{-11} m

Table 8: Summary of error signals and obtained accuracies in the power recycled configuration at 25 W input power, compared with the requirements.

7.3 Dual recycled 125 W

In dual recycled configuration the DC readout offset is added to the DARM degree of freedom and it has a value of $1 \cdot 10^{-11}$ in order to have 80 mW of carrier power reaching the dark port. The characteristics of the control filters are summarized in tab. 11. Note that the simulation of the interferometer response to laser frequency has not been simulated completely above 5 kHz. This means that the frequency stabilization control filter must include, in addition to the singularities shown in the mentioned table, also some shaping to compensate the optical one around few tens of kHz.

The signals used to control each degree of freedom are listed in tab. 12.

In the dual recycled case the DARM loop is forced to have a quite high bandwidth (475 Hz in this case) in order to properly stabilize the unstable optical spring generated by the interplay between the DC readout offset and the signal recycling cavity. Note that the computation of phase margin does not include the effect of any delay introduced by the DAQ system. The effect can be significant at these high unity gain frequencies.

Figure 7 shows the sensing noise introduced in the detector sensitivity by the longitudinal control loops. Again the MICH loop is close to the 1/10 safety factor ad even slightly above it. Any increase of sensing noise with respect to shot noise in this configuration will result in the longitudinal control not being compliant with the

D.O.F.	Control filter	UGF	Gain mar.	Ph. mar.
DARM	$207000\frac{(s+607.3)(s^2+560.7s+9.872\cdot10^4)(s^2+292.2s+1.372\cdot10^5)(s^2+839.9s+2.474\cdot10^6)}{s^2(s+1.714\cdot10^4)^2(s+1.064\cdot10^4)^2(s+11.65)^2}$	400 Hz	10 db	37 deg.
Freq.	$-2.86\cdot10^{16}\frac{(s+31.48)(s+2.151\cdot10^4)(s+2.208\cdot10^4)(s^2+7.482s+859.4)}{s^3(s+3.434e05)(s+3.715e05)(s^2+0.03484s+13.99)}$	18 kHz	13 db	33 deg.
MICH	$3041\frac{(s+11.58)(s+11.33)(s+12.34)(s+12.49)(s+13.16)(s^2+4.439s+202.4)}{s^2(s+0.06575)(s+0.04294)(s+322.3)^2(s^2+0.6643s+29.41)}$	15 Hz	7 db	26 deg.
PRCL	$-482.0\frac{(s+18.6)(s+19.61)(s+16.67)(s+29.43)^2}{s^2(s+891.9)(s+991.7)(s+0.3659)^2}$	40 Hz	13 db	34 deg.
SRCL	$239800\frac{(s+41.74)(s+48.57)^2(s^2+16.04s+1104)}{s^2(s+1899)(s+812.9)(s+0.1727)^2}$	50 Hz	10 db	31 deg.

Table 9: Control filters in the dual recycled 25 W configuration.

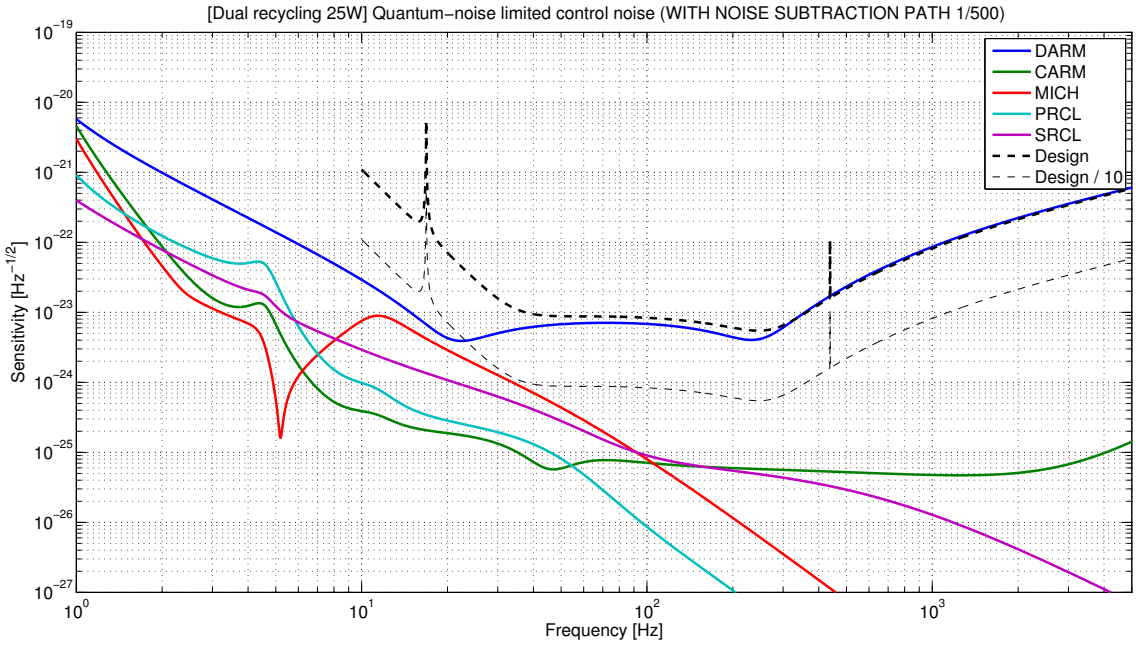

Figure 6: Sensing noise re-introduced in the detector sensitivity by longitudinal control loops in the dual recycled configuration with 25 W input power.

D.O.F.	Error signal	Accuracy	Requirement
DARM	B1_DC	$1.1 \cdot 10^{-15}$ m	$1 \cdot 10^{-15}$ m
Frequency	B2_SB3_P	0.05 mHz	7 mHz
MICH	B5_SB2_Q	$1.8 \cdot 10^{-12}$ m	$2 \cdot 10^{-12}$ m
PRCL	B2_SB1_P	1×10^{-13} m	2×10^{-11} m
SRCL	B5_SB2_P	3×10^{-14} m	2×10^{-12} m

Table 10: Summary of error signals and obtained accuracies in the dual recycled configuration at 25 W input power, compared with the requirements.

requirements.

The accuracies of the loop are summarized in tab. 12. All loops are compliant with the requirements. It can be noted that the MICH loop has a much better accuracy than the requirement. This is however necessary in order to reach a good accuracy also on DARM, due to the radiation pressure increased MICH-DARM couplings at low frequency.

8 Consequences on modulation and demodulation noises

The main gravitational channel is extracted using DC readout, therefore it is not affected by radio-frequency sideband noises, provided the OMC filtering is adequate. However all the signals used for the auxiliary degrees of freedom control are obtained with standard demodulation technique. Therefore any phase or amplitude noise of the radio-frequency sidebands will pollute these signals.

The coupling of phase and amplitude noise can be modeled with good accuracy as a cross quadrature coupling. If the Q quadrature of a signal is not perfectly zero, due to an offset or to residual RMS motion, it induces a

D.O.F.	**Control filter**	**UGF**	**Gain mar.**	**Ph. mar.**
DARM	$107000\frac{(s+607.3)(s^2+560.7s+9.872\cdot10^4)(s^2+292.2s+1.372\cdot10^5)(s^2+839.9s+2.474\cdot10^6)}{s^2(s+1.714\cdot10^4)^2(s+1.064\cdot10^4)^2(s+11.65)^2}$	475 Hz	11 db	37 deg.
Freq.	$-2.18\cdot10^{17}\frac{(s+31.48)(s+1.003\cdot10^4)(s+1.242\cdot10^4)(s^2+7.482s+859.4)}{s^3(s+8.719e05)(s+7.651e05)(s^2+0.03484s+13.99)}$	21 kHz	21 db	60 deg.
MICH	$-7.017\frac{(s+25.71)(s+22.63)(s+33.34)(s+16.28)(s+15.08)(s+12.47)(s+362.8)(s^2+15.25s+587.1)}{s^2(s+226.4)(s+145.7)(s+135.2)(s^2+1.031s+2.927)(s^2+0.7515s+26.08)}$	16 Hz	5 db	22 deg.
PRCL	$-482.0\frac{(s+18.6)(s+19.61)(s+16.67)(s+29.43)^2}{s^2(s+891.9)(s+991.7)(s+0.3659)^2}$	34 Hz	11 db	34 deg.
SRCL	$-239800\frac{(s+41.74)(s+48.57)^2(s^2+16.04s+1104)}{s^2(s+1899)(s+812.9)(s+0.1727)^2}$	45 Hz	10 db	31 deg.

Table 11: Control filters in the dual recycled 25 W configuration.

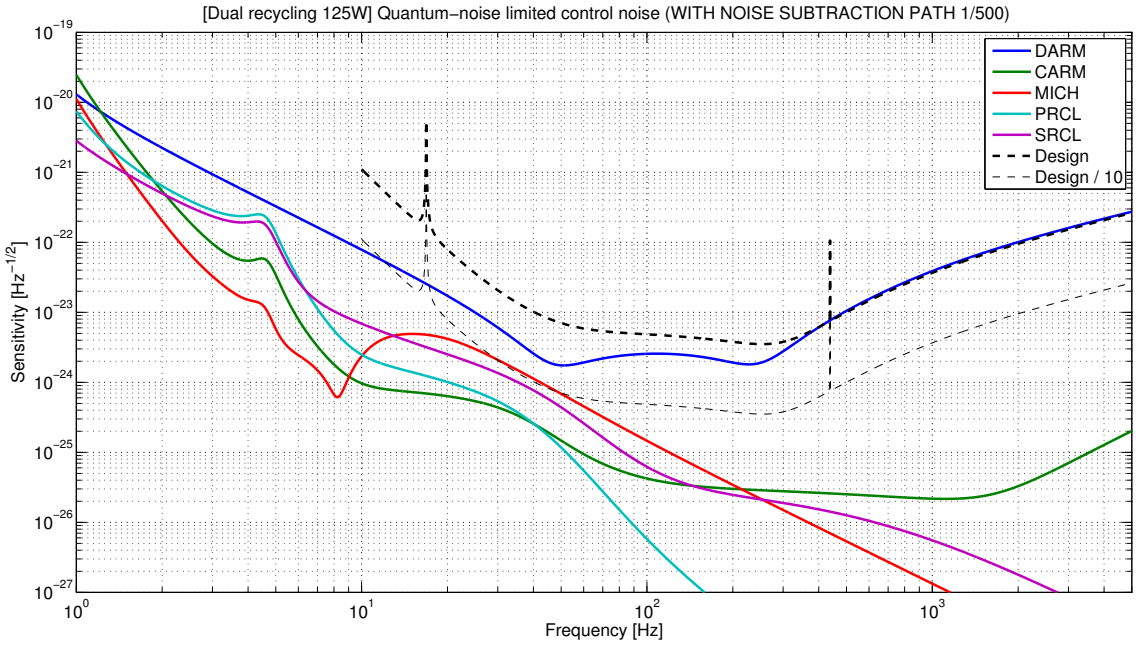

Figure 7: Sensing noise re-introduced in the detector sensitivity by longitudinal control loops in the dual recycled configuration with 125 W input power.

D.O.F.	Error signal	Accuracy	Requirement
DARM	B1_DC	$6 \cdot 10^{-16}$ m	$1 \cdot 10^{-15}$ m
Frequency	B2_SB3_P	0.09 mHz	7 mHz
MICH	B5_SB2_Q	$2.4 \cdot 10^{-14}$ m	$2 \cdot 10^{-12}$ m
PRCL	B2_SB1_P	1×10^{-14} m	2×10^{-11} m
SRCL	B5_SB2_P	3×10^{-15} m	2×10^{-12} m

Table 12: Summary of error signals and obtained accuracies in the dual recycled configuration at 125 W input power, compared with the requirements.

coupling of phase noise in the P quadrature. There is a simple proportionality relation between the size of Q signal and the level of phase noise coupling into P:

$$\tilde{n}_P(f) = \delta Q_{RMS}\, \tilde{\phi}(f) \tag{13}$$

where $\tilde{\phi}(f)$ is the spectrum of the phase noise, measured in rad/$\sqrt{\text{Hz}}$, δQ_{RMS} is the residual motion or offset in the Q quadrature and finally $\tilde{n}_P(f)$ is the resulting noise into the P quadrature. A similar equation holds for the other quadrature.

A similar coupling equation holds for the sideband amplitude noise, this time coupling each quadrature with its own RMS motion:

$$\tilde{n}_P(f) = \delta P_{RMS}\, \frac{\tilde{\delta A}(f)}{A} \tag{14}$$

where $\frac{\tilde{\delta A}(f)}{A}$ is the residual amplitude noise of the sideband at the given frequency, measured in $1/\sqrt{\text{Hz}}$ and δP_{RMS} is the residual motion or offset in the phase quadrature. A similar equation holds for the other quadrature.

From the simulations described in the previous sections, the obtained loop accuracy can be translated in residual RMS signals in each port quadrature. Each port is sensing 100 mW, therefore the reference noise level is given

Frequency	**Phase noise [rad/$\sqrt{\text{Hz}}$]**	**Relative amplitude noise [1/$\sqrt{\text{Hz}}$]**
6.3 MHz	$1.8 \cdot 10^{-6}$	$1.7 \cdot 10^{-7}$
56.4 MHz	$1.1 \cdot 10^{-6}$	$1.1 \cdot 10^{-6}$
8.4 MHz	0.27	$1.7 \cdot 10^{-7}$

Table 13: Summary of requirements for sideband amplitude and phase noise at the level of the mixer input.

by the corresponding shot noise of $1.4 \cdot 10^{-10}$ W/$\sqrt{\text{Hz}}$, as computed by Optickle. Asking the sideband phase and amplitude noise to be a factor 10 below the shot noise, one can obtain requirements on the total modulation and demodulation noises at the mixer input. Results are summarized in tab. 13, quoting only the most stringent requirement for each frequency.

9 Conclusions

The full steady state longitudinal control of the Advanced Virgo interferometer has been simulated using Optickle. The performances of the control loops in terms of control noise and accuracy has been computed, assuming each photo-diode signal is sensing 100 mW and is dominated by shot-noise, being all other sources of noise negligible. The accuracy of each loop has been computed starting from free motion of the mirrors of the order of what has been measured in Virgo, namely about 0.2 μm RMS.

Three different configurations have been simulated (power recycling only at 25 W input power, dual recycling at both 25 and 125 W). In all these configurations the longitudinal control system is compliant with both accuracy and noise requirements, provided shot noise level is not exceeded and residual motion of the mirror suspension point does not exceed the Virgo case. To obtain these results noise subtraction paths with a factor 500 of suppression are needed. This performance is of the order of magnitude of what obtained in Virgo+. Any increase of sensing noise above the shot noise level would result in the control loops not meeting the requirements of the total control noise to remain a factor 10 below the design sensitivity. All control loops are already quite at the limit in term of stability, therefore there is no more room for improvements.

To meet the accuracy requirement a careful and precise inversion of the optical matrix is needed. In the power recycling case the needed precision is not very high (about 10%) while in the dual recycled case a precision at the level of fraction of percents will be needed. This will be very challenging and would likely require an adaptive diagonalization system.

The requirement in terms of accuracy for the DARM loop have consequences on the amount of spurious power that can be tolerated in transmission of the output mode cleaner. As summarized in tab. 5, the maximum power is of the order of 0.08 mW.

Finally, the obtained accuracies allow computing requirements in term of modulation and demodulation noises, which are summarized in tab. 13.

10 Acknowledges

This research activity has been partially supported by Regione Toscana (Italy) through the program POR CreO FSE 2007-2013 of the European Community, within the project n. 18113 (ISAV).

References

[1] G. Vajente, R. Day, J. Marque, *AdV optical layout: new parameters proposal*, VIR-0377B-11 (2011) 1, 2

[2] G. Vajente, *Advanced Virgo steady state Length Sensing and Control simulation*, VIR-0449D-11 (2011) 1, 5

[3] Optickle home-page, http://ilog.ligo-wa.caltech.edu:7285/advligo/ISC_Modeling_Software 1, 9

[4] E. Tournefier, *Advanced Virgo output mode cleaner: specifications*, VIR-0071A-08 (2008) 7

[5] R. Gouaty, E. Tournefier, B. Mours, P. Mugnier, L. Rolland, *Advanced Virgo output mode cleaner: Revised specifications*, VIR-0037A-11 7

[6] J. Marque, G. Vajente, *Proposal of an alternative design of the OMC to improve filtering performance*, VIR-0713A-11 7

[7] G. Vajente, *Advanced Virgo Length Sensing and control: Double demodulation vs Single demodulation*, VIR-0069B-08 10

[8] B. Gustavsen and A. Semlyen, *Rational approximation of frequency domain responses by vector fitting*, IEEE Trans. Power Delivery, vol. 14, no. 3, pp. 1052-1061, July 1999 10

[9] B. Swinkels, E. Campagna, G. Vajente, L. Barsotti and M. Evans, *Longitudinal noise subtraction: the alpha-, beta- and gamma-technique*, VIR-0050A-08 10